Oceanologia (2019) 61, 350—367

Available online at www.sciencedirect.com

ScienceDirect

journal homepage: www.journals.elsevier.com/oceanologia/

ORIGINAL RESEARCH ARTICLE

Laboratory study of suspended sediment dynamics over a mildly sloping sandy seabed

Barbara Stachurska *, **Ryszard Staroszczyk**

Institute of Hydro-Engineering, Polish Academy of Sciences, Gdańsk, Poland

Received 9 July 2018; accepted 29 January 2019
Available online 21 February 2019

KEYWORDS
Sediment dynamics;
Sloping seabed;
Bed ripples;
Wave bottom boundary layer;
Particle image velocimetry

Summary This paper presents the results of laboratory measurements of suspended sediment movement induced by regular non-linear water waves propagating over a mildly sloping sandy seabed covered with ripples. The measurements conducted in a water flume were carried out by applying the technique of particle image velocimetry (PIV). The aim of those experiments was to investigate near-bed velocities of sediment particles under controlled surface wave conditions. In particular, horizontal and vertical profiles of sand grain velocities were measured, and some comparisons between the measured and theoretically-predicted quantities were carried out. A number of selected wave cases were examined, for which the Ursell number ranged from 18 to 39, and the sediment grain mobility numbers varied between 12 and 26. For these flow conditions, the near-bed layer of intense sediment grain movements had a thickness of about 2—3 ripple heights. The maximum horizontal sediment velocities measured over ripple crests were about twice as large as those over ripple troughs. Vertical sediment velocities above ripple crests and troughs were similar, amounting to about 1/4 to 1/3 of horizontal velocities over ripple crests. The detailed quantitative results obtained in the flume can help validate other experimental techniques and can be useful in testing numerical models for simulating surface wave-induced sediment dynamics.

1. Introduction

When deep water waves approach a seashore, they enter a shoaling region (see Fig. 1), in which they undergo a significant transformation that gives rise to a complex oscillatory motion of water particles and generates water currents near the seabed. As surface waves enter a region of gradually decreasing water depth, their height and steepness grow,

* Corresponding authors at: Institute of Hydro-Engineering, Polish Academy of Sciences, Gdańsk, Poland.
E-mail address: b.stachurska@ibwpan.gda.pl (B. Stachurska).
Peer review under the responsibility of Institute of Oceanology of the Polish Academy of Sciences.

ELSEVIER Production and hosting by Elsevier

https://doi.org/10.1016/j.oceano.2019.01.006

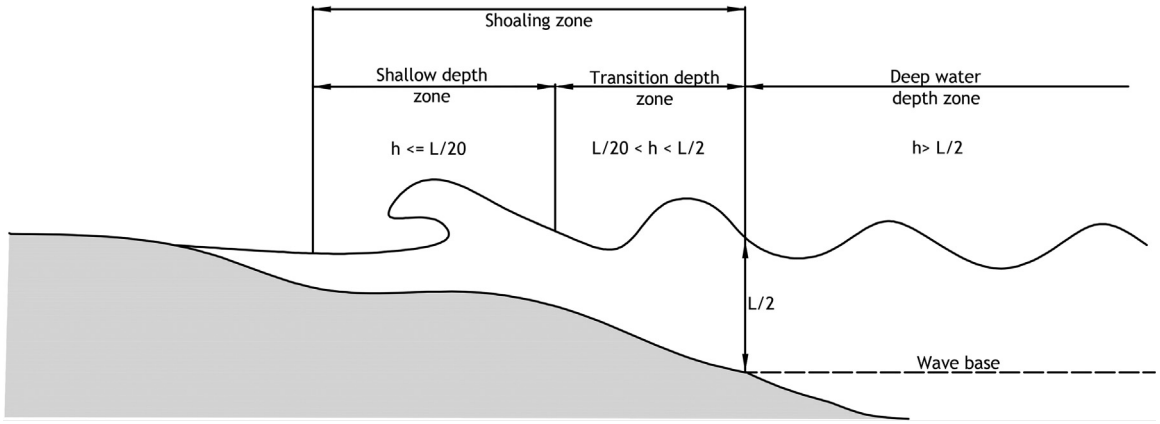

Figure 1 Schematic diagram of a coastal zone profile (*h* denotes water height, and *L* denotes deep-water wavelength).

resulting in increasing orbital velocities of water particles across the water column. The increasing water velocities near a sandy seabed increase shear stresses exerted by oscillating water on sediment grains, which intensifies all dynamic processes occurring in a near-bed layer of turbulent flow, such as the formation, evolution and migration of bed ripples, the entraining of sand grains into suspension, and onshore/offshore transport of sediment along the bed. Such complex phenomena have been investigated, both empirically and theoretically, for decades (Alsina et al., 2012; Bagnold, 1946; Doering and Baryla, 2002; Grant and Madsen, 1982; Inman and Bowen, 1962; Sato et al., 1984), but it seems that, despite the vast literature, the fundamental mechanisms underlying the motion of sediment particles over the seabed are not yet fully understood. The development of modern experimental techniques offers new opportunities for observation and measurement of fundamental mechanisms occurring on small spatial scales near the seabed. One such modern technique is particle image velocimetry (PIV).

The PIV technique is based on a digital analysis of images of tracer particles seeded in water and observed within a thin sheet of fluid lit by laser light (Willert and Gharib, 1991). Originally, this technique was intended for use in one-phase fluid flows, and has been successfully used in many problems of hydrodynamics and related disciplines. Its application to two-phase fluid flows, and such is the flow of sediment particles suspended in water, can still be regarded as a novel approach. One of the first attempts to use the PIV method in experiments involving the motion of sandy sediments induced by water waves was due to Ahmed and Sato (2001). Van der Werf et al. (2007) applied this experimental method for the detailed investigation of water vortex generation above seabed ripples and their effect on the ejection of sand grains into the water column. Yang et al. (2011) developed an approach that makes it possible to simultaneously determine the velocity fields of water and sediment particles by using fluorescent seed particles. Further, Umeyama (2012) applied the PIV technique to measure particle trajectories due to surface waves propagating in water of finite depth. More recently, Stachurska and Staroszczyk (2016) used the PIV method to investigate the motion of sediment particles in the vicinity of a rippled bed for surface wave-generated flows in water of constant depth.

This paper is a continuation and extension of research reported in the latter paper (Stachurska and Staroszczyk, 2016). Thus, wave-generated flows in water of slightly varying depth are now investigated, that is, the region denoted in Fig. 1 as the 'transition zone' is considered. For this purpose, sediment motion generated by non-linear (Stokes) waves propagating over a bed inclined at a constant angle of 2% with a system of well-developed ripples was analyzed experimentally in a water flume. The objective of the laboratory PIV measurements was to investigate in detail the dynamics of sediment particles under controlled surface wave conditions. The main point of interest was to determine the velocities of sand particles near a rippled bed. In particular, the vertical profiles of horizontal and vertical sediment velocities over ripple crests and ripple troughs were measured, and the variation of sediment velocities in the horizontal direction along the bed ripples was investigated. Moreover, a number of parameters characterizing sediment dynamics were determined, including the grain mobility number, the Shields parameter and the thickness of the turbulent near-bed layer, commonly referred to as the wave bottom boundary layer (WBBL). Some of the results from the flume measurements were compared with theoretical estimations based on analytical formulae available in the literature.

The experimental results obtained in the laboratory and described in this study give insights into the complex mechanisms taking place in the immediate vicinity of sandy ripples in water-induced flows. The quantitative results can be used to validate other experimental techniques (especially those to be applied on larger scales in the field), and they can also be useful in testing numerical models developed to simulate sediment behaviour in surface wave-induced flows.

The paper is organized as follows. Section 2 provides some basic theoretical background and introduces some parameters used throughout the paper. Section 3 describes the experimental setup and the methodology of measurements and data post-processing. Section 4 presents detailed results obtained during the laboratory work, including the vertical and horizontal profiles of sediment particle velocities. Section 5 is devoted to the comparisons of the measured data with theoretical estimations, and Section 6 presents the most important conclusions from the laboratory experiments.

2. Theoretical framework

Before the presentation and discussion of experimental results obtained in the flume, some basic theoretical framework is given below.

2.1. Description of surface waves

The laboratory experiments were carried out for surface waves with parameters (the wave length and height) corresponding to those of finite-amplitude non-linear waves propagating in shallow water. Hence, it was assumed that waves generated in the flume during the experiments can be approximated by the second-order Stokes theory (Fenton, 1990). Accordingly, in a rectangular coordinate system Oxz with the horizontal x-axis assumed along the wave propagation direction and the vertical z-axis pointing upwards and its origin assumed at the still water surface, the water particle horizontal and vertical velocity components u and v respectively, for waves travelling over a horizontal bottom, are given by:

$$u = \frac{HgT}{2L}\frac{\cosh\left(\frac{2\pi(z+h)}{L}\right)}{\cosh\left(\frac{2\pi h}{L}\right)}\cos\left(\frac{2\pi x}{L}-\frac{2\pi t}{T}\right) + \frac{3}{4}\left(\frac{\pi H}{L}\right)^2 c\frac{\cosh\left(\frac{4\pi(z+h)}{L}\right)}{\sinh^4\left(\frac{2\pi h}{L}\right)}\cos\left(\frac{4\pi x}{L}-\frac{4\pi t}{T}\right), \quad (1)$$

$$v = \frac{HgT}{2L}\frac{\sinh\left(\frac{2\pi(z+h)}{L}\right)}{\sinh\left(\frac{2\pi h}{L}\right)}\sin\left(\frac{2\pi x}{L}-\frac{2\pi t}{T}\right) + \frac{3}{4}\left(\frac{\pi H}{L}\right)^2 c\frac{\sinh\left(\frac{4\pi(z+h)}{L}\right)}{\sinh^4\left(\frac{2\pi h}{L}\right)}\sin\left(\frac{4\pi x}{L}-\frac{4\pi t}{T}\right). \quad (2)$$

In the above equations, L denotes the surface wave length, H is the wave height, t is time, T is the wave period, h is the still water depth, c is the wave phase velocity (celerity) and g stands for the gravitational acceleration. The derived quantities, ω and k, representing the angular frequency and the wave number, are also used in the theoretical description. These are defined by the formulae:

$$\omega = \frac{2\pi}{T}, \quad k = \frac{2\pi}{L}, \quad c = \frac{\omega}{k}. \quad (3)$$

The quantities ω, k and h are related through the dispersion relation:

$$\omega^2 = gk\tanh kh. \quad (4)$$

In order to determine whether, for given wave parameters, we deal with Stokes or cnoidal wave regimes, an Ursell number (Ursell, 1953) defined by the formula

$$U_r = \frac{H}{h_s}\left(\frac{L_s}{h_s}\right)^2 \quad (5)$$

was calculated, where L_s and h_s denote, respectively, the wave length and water depth at a given location over the sloping bed. It was found that for the waves generated in the flume during our experiments, the Ursell number ranged between the values of around 18 and 39, see Table 1 in Section 3. According to Fenton (1990) and Hedges (1995), the latter range corresponds indeed to the Stokes wave regime (the cnoidal wave theory is applicable for $U_r \geq 40$).

To characterize the water flow regime near the bed, the Reynolds number defined by the relation

$$Re = \frac{u_0^2}{\omega\nu} \quad (6)$$

was calculated, where u_0 is the amplitude of the horizontal velocity of water near the bed, and ν is the kinematic viscosity of water (equal to 10^{-6} m^2 s^{-1}). The values of the Reynolds number calculated for our laboratory conditions are listed further in Table 1 in the next section. They range, approximately, between 0.9×10^4 and 2.1×10^4, which indicates that the flow near the flume bed was turbulent, and the laboratory conditions were close to those encountered in the field, for which the Reynolds numbers commonly have the values of order 10^5 (Nielsen, 1992).

2.2. Relations describing sediment dynamics

One of the key parameters in mechanics of sediment transport is the so-called Shields parameter θ which describes the ratio of the water flow-generated shear force acting on a sediment particle resting on the bed to its own weight in water. The value of this parameter allows us to estimate, in an approximate manner, the sediment movement regime in the vicinity of a rough bed. In the literature, the Shields parameter is commonly defined on the assumption that the bed grain roughness equals $2.5d_{50}$ (where d_{50} denotes the median grain diameter). In this case, the Shields parameter, denoted then as $\theta_{2.5}$, is given by the following relation (Nielsen, 1992):

$$\theta_{2.5} = \frac{\frac{1}{2}f_{2.5}(A\omega)^2}{(s-1)gd_{50}}. \quad (7)$$

Table 1 Parameters of surface waves investigated in the experiments. *Notations*: h and h_s are deep and shallow water depths, respectively, H is the wave height, T is the wave period, L and L_s are wave lengths in deep and shallow water, respectively, U_r are Ursell numbers, Re are Reynolds numbers, and ψ are mobility numbers.

Case	h [m]	h_s [m]	H [m]	T [s]	L [m]	L_s [m]	U_r	Re	ψ
A	0.35	0.185	0.08	1.0	1.4	1.2	17.6	8.6×10^3	12.7
B			0.10	1.0			22.0	1.5×10^4	21.6
C			0.11	1.0			24.2	1.8×10^4	26.2
G			0.06	1.4	2.3	1.8	29.5	1.1×10^4	11.6
H			0.08	1.4			39.4	2.1×10^4	24.6

The parameter $f_{2.5}$ entering the above equation denotes the grain roughness friction factor and is determined by the following formula (Nielsen, 1992):

$$f_{2.5} = \exp\left[5.213\left(\frac{2.5d_{50}}{A}\right)^{0.194} - 5.977\right]. \tag{8}$$

In Eqs. (7) and (8), A is the orbital displacement amplitude of the fluid immediately above the bed boundary layer and s is the ratio of the densities of the sediment grain and water ($s = 2.65$ for quartz sand).

Based on the observations, it is usually assumed that grains at the bed start to move at $\theta_{2.5} \sim 0.05$, sand ripples develop and remain stable at $\theta_{2.5} \sim 0.2 \div 0.3$, and at $\theta_{2.5} \sim 0.8 \div 1.0$ all bedforms are destroyed and a mass sediment movement occurs (Nielsen, 1992; Ostrowski, 2004). As will be shown in Section 5, the values of the Shields parameter $\theta_{2.5}$ for flow conditions investigated in the flume experiments varied from about 0.1 to about 0.3, that is, within the range at which sandy ripples develop at the bed and remain stable.

An alternative dimensionless parameter that is often used for measuring forces exerted by water waves on sediment particles is the mobility number, ψ, defined by

$$\psi = \frac{(A\omega)^2}{(s-1)gd_{50}}. \tag{9}$$

By comparing Eqs. (7) and (9) it can be noted that the two dimensionless quantities, $\theta_{2.5}$ and ψ, are related by the simple formula

$$\theta_{2.5} = \frac{1}{2} f_{2.5}\psi. \tag{10}$$

The roughness of the sandy bed, even if there are no ripples thereon, considerably affects the oscillatory flow of water in the water column close to the bed. This is caused by the development of a turbulent boundary layer, which, if due to the propagation of surface waves, is often referred to as the wave bottom boundary layer (WBBL). There are a number of approximate analytic formulae proposed in the literature (e.g. Fredsoe, 1984; Fredsoe and Deigaard, 1992; Grant and Madsen, 1979) for the estimation of the WBBL thickness in terms of parameters defining a surface wave and the properties of the rough bed. In this work, for a bed which is covered by a system of ripples (i.e. is not flat), we apply an approach due to Nielsen (1992), by which the WBBL thickness, δ, is given by:

$$\delta = \frac{1}{2}\frac{u}{\omega} f_w, \tag{11}$$

where u is the horizontal velocity of water at the top of the boundary layer (the so-called free-stream velocity), and f_w denotes a quantity known as the wave friction factor. To calculate the latter quantity, the value of the Shields parameter defined above by Eqs. (7) and (8) is used. Accordingly, at first the hydraulic roughness of the rippled bed, r, is estimated by applying the formula (Nielsen, 1992):

$$r = \frac{8\eta_r^2}{\lambda_r} + 170d_{50}\sqrt{\theta_{2.5} - 0.05}, \tag{12}$$

in which η_r and λ_r denote the characteristic ripple height and length, respectively. Assuming that the bed is hydraulically rough (implying turbulent flow in the boundary layer), the wave friction parameter f_w is defined in terms of the roughness parameter r by the equation:

$$f_w = \exp\left[5.5\left(\frac{r\omega}{u}\right)^{0.2} - 6.3\right]. \tag{13}$$

Given the value of f_w calculated from relation (13), the boundary layer thickness δ can be estimated from Eq. (11). The values of δ predicted by the theory for the surface waves investigated in this work will be compared with those observed in the flume experiments in Section 5.2.

In order to evaluate from Eq. (12) the bed roughness r, the bed ripple length and height are needed. For regular waves, the ripple length is calculated from the following formula (Nielsen, 1981):

$$\frac{\lambda_r}{A} = 2.2 - 0.345\psi^{0.34}, \tag{14}$$

which is valid for the mobility number range $2 < \psi < 230$. The characteristic ripple height, in turn, is given by the relation

$$\frac{\eta_r}{A} = \max\{0.275 - 0.022\psi^{0.5}, 0\}. \tag{15}$$

Alternatively, the ripple height can be determined in terms of the Shields parameter $\theta_{2.5}$ by applying the formula

$$\frac{\eta_r}{\lambda_r} = 0.182 - 0.24\theta_{2.5}^{1.5}. \tag{16}$$

Since the laboratory experiments presented in this work focus on the measurement of suspended sediment particle velocities, it is of interest to evaluate the settling velocity of a single particle descending in fluid in rest (this velocity is determined from the condition that the fluid drag force acting on the particle balances the gravity force). From among a number of formulae which are available in the literature, we chose an empirical one proposed by Onoszko (1965):

$$v_s = 9.45(s-1)^{0.8} d_{50}, \tag{17}$$

in which v_s is in units [m s^{-1}] and d_{50} in [m]. The above-defined settling velocity can be treated as a characteristic scale for the vertical sediment particle velocities measured in the flume experiments.

3. Experimental setup and data processing

The experiments were carried out in a wave flume belonging to the Institute of Hydro-Engineering of the Polish Academy of Sciences in Gdańsk, Poland. The facility is 64 m long, 0.6 m wide and 1.4 m deep. Water waves are generated in the flume by a programmable piston-type wave maker. The experiments described in this work were carried out for the still water depth $h = 0.35$ m. For the purpose of the experiments, an inclined bottom section with a slope of 2% and a length of 20.0 m was inserted into the flume (see Fig. 2). The inclined bottom started at a distance of 21.25 m from the wave generator. Natural sand, taken from a beach at a village of Sobieszewo (part of the Gdańsk agglomeration), was used in the experiments. The median diameter of sand grains, determined by sieve analysis, was $d_{50} = 0.257$ mm. The sand was placed in a tray (cuvette), which was mounted on the sloping bottom at a depth of about

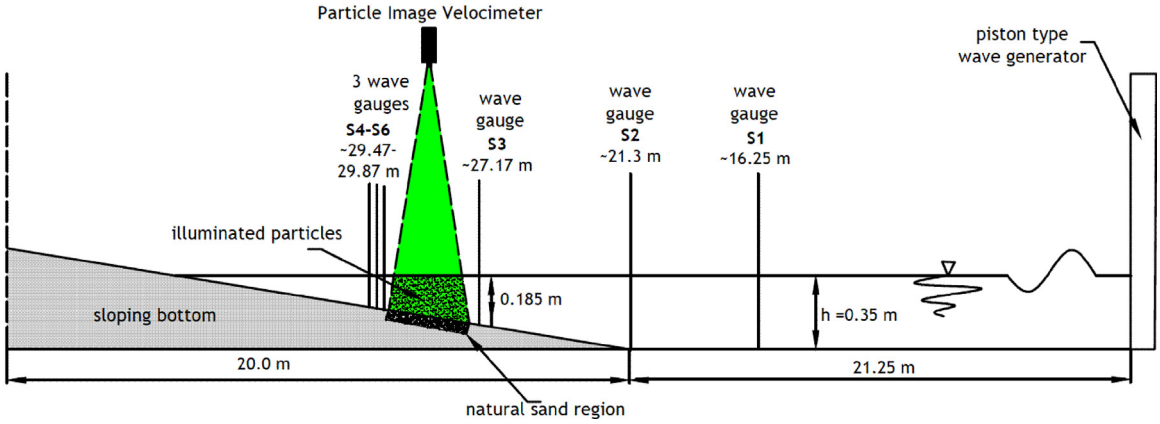

Figure 2 Experimental setup.

0.185 m, that is, at approximately 1/2 of the still water level measured relative to the flat horizontal section of the flume bottom. This particular location of the sand tray was chosen to ensure full transformation (steepening and shortening) of waves coming from the constant-depth section of the flume, with wave parameters selected in such a way that near-breaking wave conditions occurred for the highest waves considered in the experiments.

A PIV laser beamer was mounted over the middle part of the sand tray, and a high-definition video camera was placed in front of the glazed vertical sidewall of the flume to record laser light-illuminated sediment particles (see Fig. 3). The PIV system used in the experiments was supplied by LaVision. The sampling frequency (at which pairs of PIV images were recorded) was 15 Hz, with an inter-frame separation time in each pair of frames ranging from 400 to 2000 μs. Successive images of sediment particle distributions were recorded by a high-speed CCD camera Imager Pro HS 500 with a sensor spatial resolution of 1280 px × 1024 px at 520 fps (frames per second). The size of the measurement window was approximately 20 cm × 17 cm. The PIV images were post-processed by the PIVlab1.4 software for MATLAB (Thielicke and Stamhuis, 2014), which uses cross-correlation to calculate vector fields between two successive frames. Spurious spikes (outliers) in velocity distributions were detected by the so-called local median filter method (based on a window of 3 × 3 grid points). Typically, the PIV technique requires seeding (small tracer particles suspended in a fluid), but it turned out in the course of the experiments that the fine sand particles reflected the laser light sufficiently well, so artificial seeding was not necessary.

Prior to the PIV measurements, water waves were generated in the flume for approximately 30 min, so that sand ripples developed on the bed and reached a state of equilibrium for given surface wave conditions, with ripple crests aligned in parallel to form a very regular pattern. The

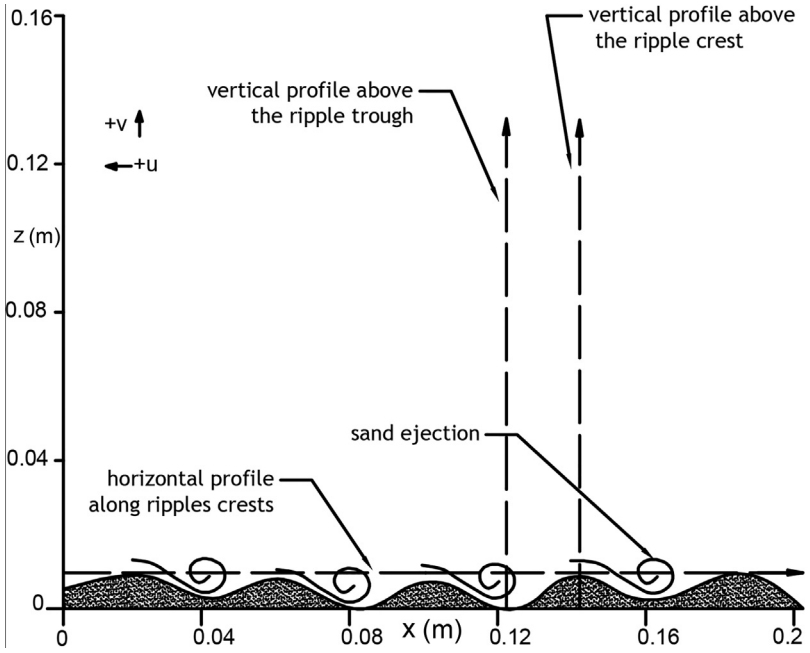

Figure 3 Vertical and horizontal profiles.

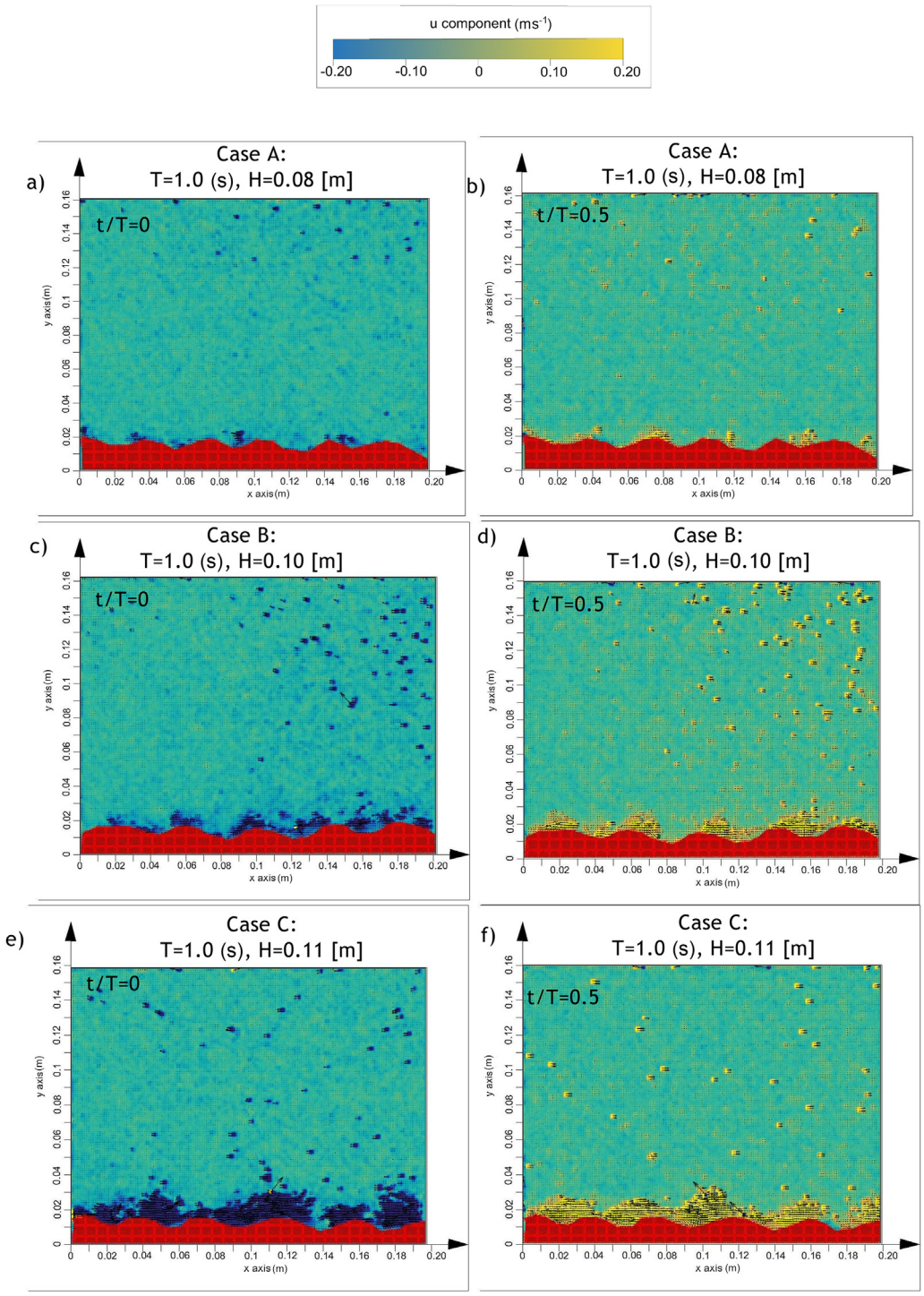

Figure 4 Instantaneous horizontal sediment velocity fields over a rippled bed for three cases of the wave height H and the wave period T = 1.0 s.

geometry of the ripples (their length and height) was measured along the lateral glass walls manually with a ruler, so the measurements were accurate to within 1 mm.

In order to record changes in the water free surface elevation, a system of six wave gauges (denoted as S1 to S6 in Fig. 2) was used. The gauges were placed near the middle of the horizontal bottom, at the beginning of the slope and directly behind the sand tray, as indicated in Fig. 2. The analysis of data recorded by these gauges showed that the distortion and damping of surface waves caused by the presence of the lateral walls of the channel were negligibly small, so the flow could be regarded as two-dimensional.

Before the proper experiments started, a series of preliminary test runs with various combinations of surface wave parameters was conducted to identify those cases in which

systems of well-developed and stable (i.e. not migrating) bed ripples were formed, no-breaking of waves took place, and no excessive vibrations of the inclined bed (which cause errors in measurements) occurred. Five of the cases tried in the preliminary tests were selected for detailed examination. These cases included waves of two different periods T, one corresponding to a medium-length wave and the other to a long wave. The maximum heights H of these two waves chosen for experiments were the largest for which the waves did not break (those higher by 1 cm broke over the sloping section of the bed). The three remaining wave cases, with smaller wave heights, were used for comparisons. The five cases selected for presentation, thereafter labelled A, B, C, G and H, are defined in Table 1 in terms of wave period T, wavelength L and wave height H. In the table, also the values of the Ursell number U_r defined by Eq. (5), the wave Reynolds number Re defined by (6), and the mobility number ψ given by relation (9) are listed for reference in the table.

4. Experimental results

In this section, the results of the laboratory tests in the flume are presented, with the five cases of surface waves investigated experimentally defined in Table 1. In the experiments, the focus was on measuring the velocities of sand particles suspended in water near the rippled bed. The results obtained in the flume are illustrated by means of velocity profiles, showing the variation of both components of the sediment grain velocity vector along an either vertical or horizontal direction. The profiles used for illustration are defined in Fig. 3. One of the two vertical profiles is located over a ripple crest, and the other is loced over a ripple trough, with the zero z-coordinates in both profiles assumed at the ripple trough level. The horizontal profile is located along a line parallel to the bed and passing through the top of the highest ripple in the PIV image window (which covered about five ripple lengths). The zero coordinate of this profile

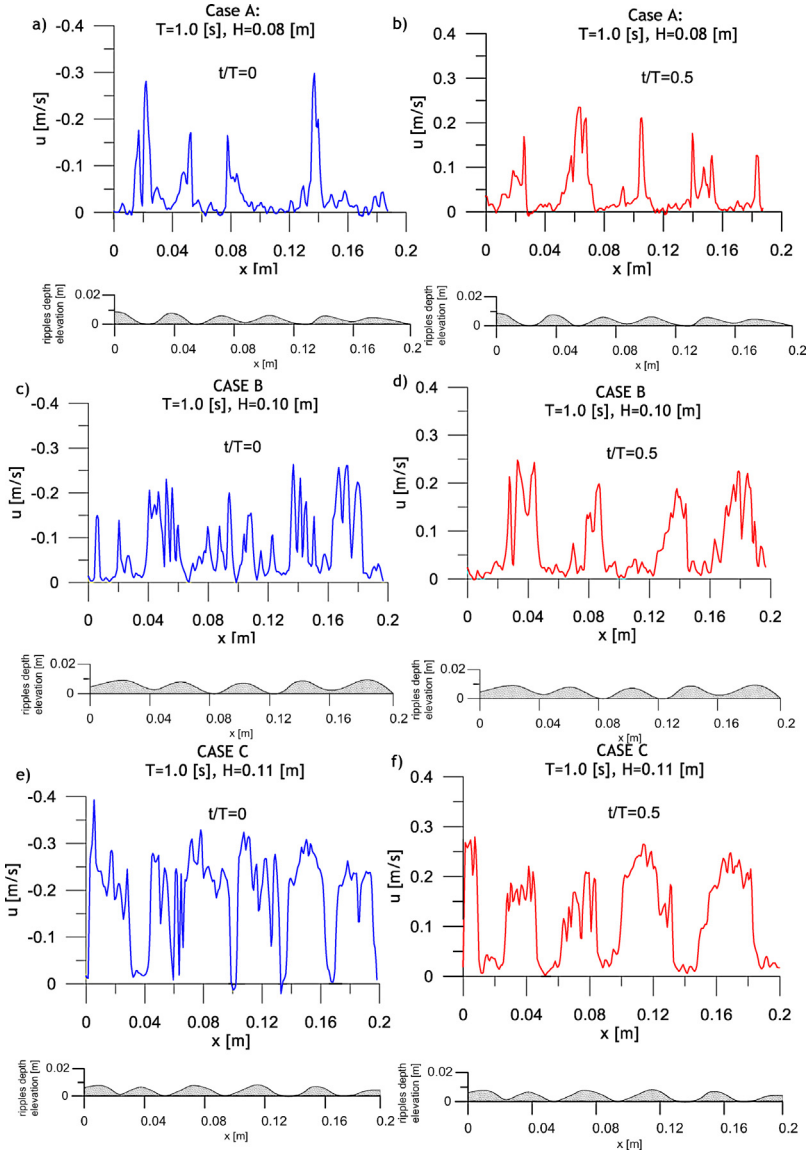

Figure 5 Instantaneous horizontal velocities of sediment grains along the horizontal profile over the bed ripples for three values of the wave height H and the wave period $T = 1.0$ s, at wave phases $t/T = 0$ (wave trough) and $t/T = 0.5$ (wave crest).

was assumed at the left side of the window, as shown in the figure.

The results of PIV measurements are presented separately for the waves of a period T = 1.0 s (cases A, B and C defined in Table 1) and the longer waves of a period T = 1.4 s (cases G and H).

4.1. Sediment velocities due to surface waves of the period T = 1.0 s

The PIV images of the instantaneous horizontal velocities of sediment particles for the three cases A, B and C are shown in Fig. 4. The images on the left correspond to the instant of a wave trough passage (t/T = 0) over the middle of the measurement window, while the images on the right illustrate the velocities at the passage of a surface wave crest (t/T = 0.5) over the same point.

The following figures illustrate sediment velocity profiles measured by the PIV technique. Fig. 5 shows plots of horizontal sediment velocities along the horizontal profile for three different values of the wave height H. Under each plot, there is the corresponding profile of bed ripples that developed under given wave conditions. The characteristics of the ripples are provided in Section 5.2. It is seen that despite the scatter in the data, the measured velocities reflect well the phenomenon of increased sediment velocities above ripple crests compared to those above ripple troughs. The case of H = 0.08 m, illustrated in Fig. 5a and b, shows that instantaneous sand particle velocities varied between -0.29 m s^{-1} during surface trough transition to 0.25 m s^{-1} during the wave crest transition. The corresponding velocities for the case H = 0.10 m were about $\pm$0.26 m s^{-1} (see Fig. 5c and d), whereas for the highest wave H = 0.11 m the measured velocities ranged from about -0.40 to 0.28 m s^{-1} (Fig. 5e and f), depending on the surface wave phase.

Fig. 6 presents the vertical distributions of instantaneous horizontal sediment velocities measured along a profile located on a ripple crest (see Fig. 3) for the three wave heights considered. It can be seen that similar, quasi-symmetric sediment velocity patterns occur in all three cases, with velocity magnitudes $|u_s|$ in the near-bed turbulent layer of much larger than those in the water column above. The magnitudes of near-bed sediment velocities, at both wave trough (t/T = 0 blue lines) and wave crest ($t/T = 0.5$, red lines) passages, increase with the wave height, as expected, though this increase, with the wave height H, can be considered as moderate. For instance, for the wave height $H = 0.08$ m (Fig. 6a), the measured sediment velocities vary between $u_s = -0.21$ m s^{-1} and u_s = +0.22 m s^{-1}, for $H = 0.10$ m (Fig. 6b) they vary between the values of about $\pm$0.25 m s^{-1}, and finally, for $H = 0.11$ m (Fig. 6c), they vary between $u_s = -0.32$ m s^{-1} and u_s = +0.27 m s^{-1}. One can expect some asymmetry in near-bottom sediment velocities (differences between the velocity magnitudes at wave trough and crest passages) that increase with the wave height, and this effect is indeed observed in Fig. 6c for the highest wave $H = 0.11$ m. The asymmetry results from the fact that, for steep non-linear waves propagating in shallow water, the wave trough passage lasts longer than the crest passage phase, so there is more time for sediment particles to catch up with water during its oscillatory flow. This explains why the most intense movement of sediment occurs during the passage of wave troughs. It is also seen in the plots that the thickness of the near-bed layer of intense sediment movement is significantly affected by the wave height H, increasing by a factor of about three between the smallest and highest waves illustrated in the figure.

Corresponding to Fig. 5 are the plots in Fig. 7, showing variations in vertical sediment velocities along the horizontal profile over the bed ripple crests. The case of $H = 0.08$ m, illustrated in Fig. 7a and b, shows that sand particle velocities varied from 0.04 m s^{-1} to -0.03 m s^{-1} during a surface trough passage and from 0.08 m s^{-1} to -0.03 m s^{-1} during a wave crest passage. The analogous velocities for the case $H = 0.10$ m changed from about 0.05 m s^{-1} to -0.04 m s^{-1} during a wave trough passage (see Fig. 7c), and from 0.07 m s^{-1} to -0.03 m s^{-1} during a crest passage (Fig. 7d).

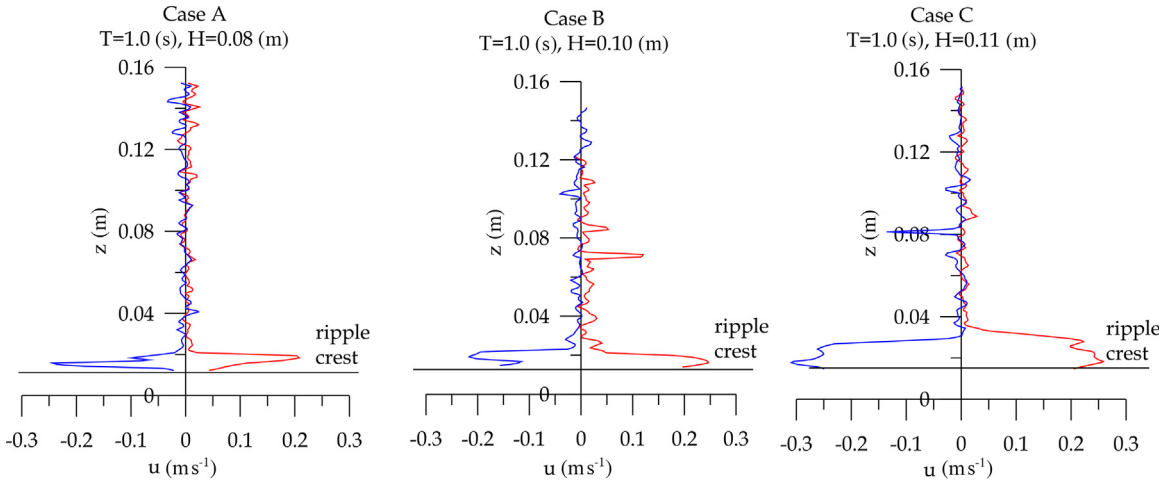

Figure 6 Instantaneous horizontal velocities of sediment grains along the vertical profile over a ripple crest for three values of the wave height H and the wave period $T = 1.0$ s, at wave phases $t/T = 0$ (wave trough passage, blue lines) and $t/T = 0.5$ (wave crest passage, red lines). (For interpretation of the references to color in this figure legend, the reader is referred to the web version of this article.)

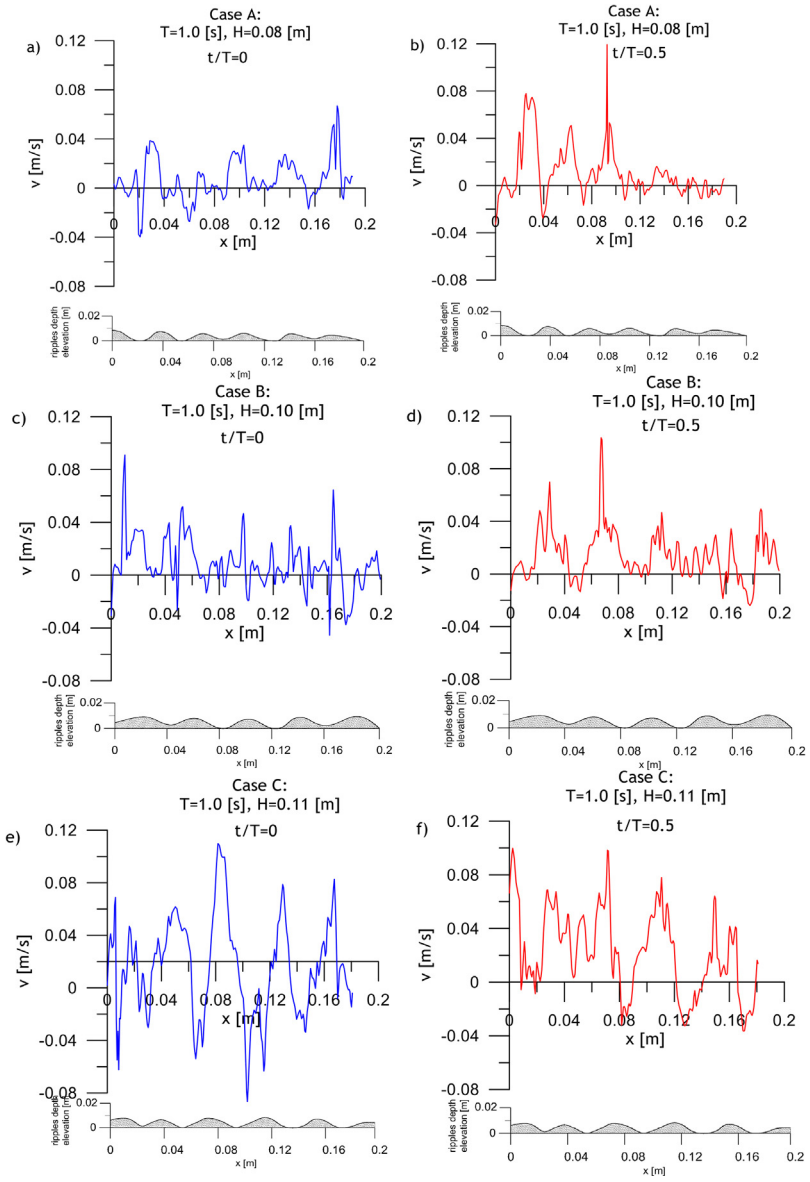

Figure 7 Instantaneous vertical velocities of sediment grains along the horizontal profile over the bed ripples for three values of the wave height H and the wave period $T = 1.0$ s, at wave phases $t/T = 0$ (wave trough) and $t/T = 0.5$ (wave crest).

For the highest wave $H = 0.11$ m, the measured horizontal velocities ranged from about 0.10 m s^{-1} to -0.08 m s^{-1} during a wave trough passage (Fig. 7e), and from 0.09 m s^{-1} to -0.04 m s^{-1} during a crest passage (Fig. 7f).

The plots in Fig. 8 illustrate the distributions of instantaneous vertical sediment velocities measured along a vertical profile located over a ripple crest (see Fig. 3) for the three wave heights considered. By comparing the plots in Figs. 6 and 8, it can be noted that the magnitudes of vertical velocities of sediment grains in the wave bottom boundary layer are about 1/3 of their horizontal counterparts. It can be observed again (see Fig. 6) that the wave height considerably affects the thickness of the near-bed turbulent layer of intense sediment movement, increasing it by a factor of about three between the smallest and the highest waves. Some asymmetry in the near-bed velocities can also be noticed, especially apparent for the highest wave illustrated in Fig. 8c.

The plots in Figs. 6 and 8 illustrate sediment velocity distributions along a vertical profile located over the top of a ripple crest. The six plots in Fig. 9 display corresponding velocity distributions for a profile located over a bed ripple trough (see Fig. 3). The upper row of plots shows horizontal components for the three wave height cases, and the lower row shows the vertical components of the velocity vector. Comparing Figs. 6 and 9, one can note that the measured magnitudes of the horizontal velocities of sediment grains immediately over ripple troughs are smaller than those over ripple crests and the relative velocity reduction decreases with the turbulent boundary layer thickness. Hence, for the

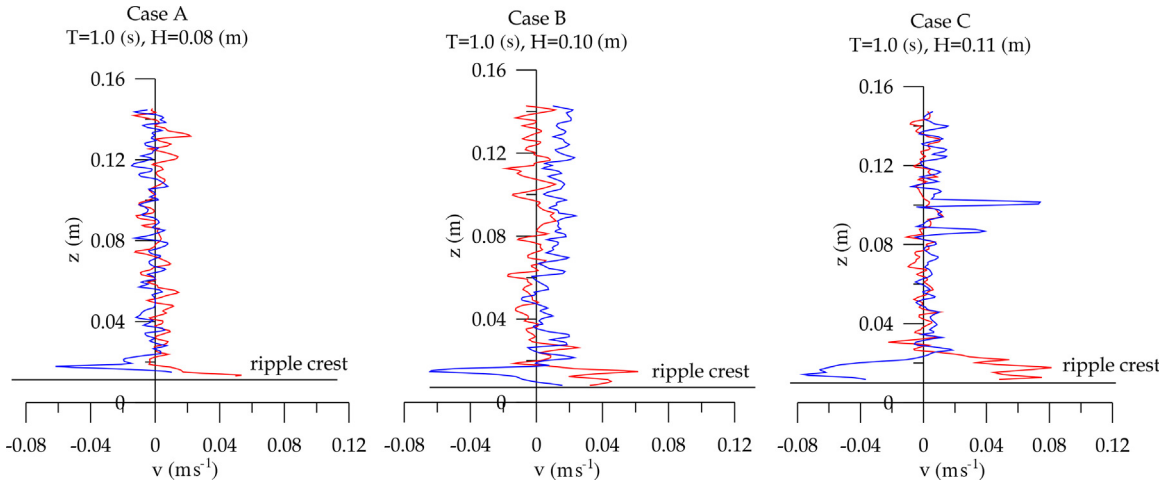

Figure 8 Instantaneous vertical velocities of sediment grains along a vertical profile over a ripple crest for three values of the wave height H and the wave period $T = 1.0$ s, at wave phases $t/T = 0$ (wave trough transition, blue lines) and $t/T = 0.5$ (wave crest transition, red lines). (For interpretation of the references to color in this figure legend, the reader is referred to the web version of this article.)

thinner layer (case A), the velocities over the ripple trough are approximately half of those over the crest, whereas for the thicker layer (case C) the near-bed horizontal velocities are reduced by about 30%. A different pattern is observed for the vertical velocities (see Fig. 8), since the magnitudes of near-bed sediment velocities over ripple crests and troughs are similar, irrespective of the wave height (and hence of the bottom boundary layer thickness).

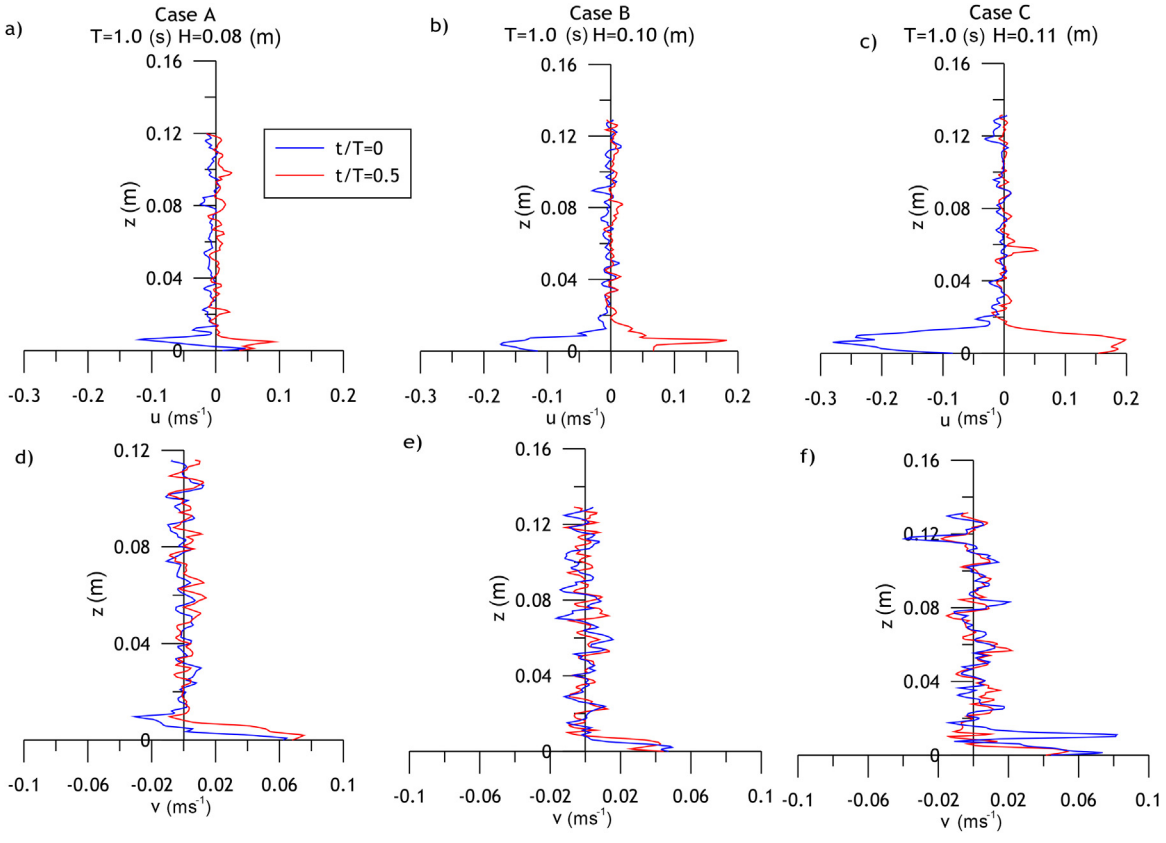

Figure 9 Instantaneous horizontal (plots a–c) and vertical (d–f) sediment velocities along a vertical profile over a ripple trough for three values of the wave height H and the wave period $T = 1.0$ s, at wave phases $t/T = 0$ (wave trough transition, blue lines) and $t/T = 0.5$ (wave crest transition, red lines). (For interpretation of the references to color in this figure legend, the reader is referred to the web version of this article.)

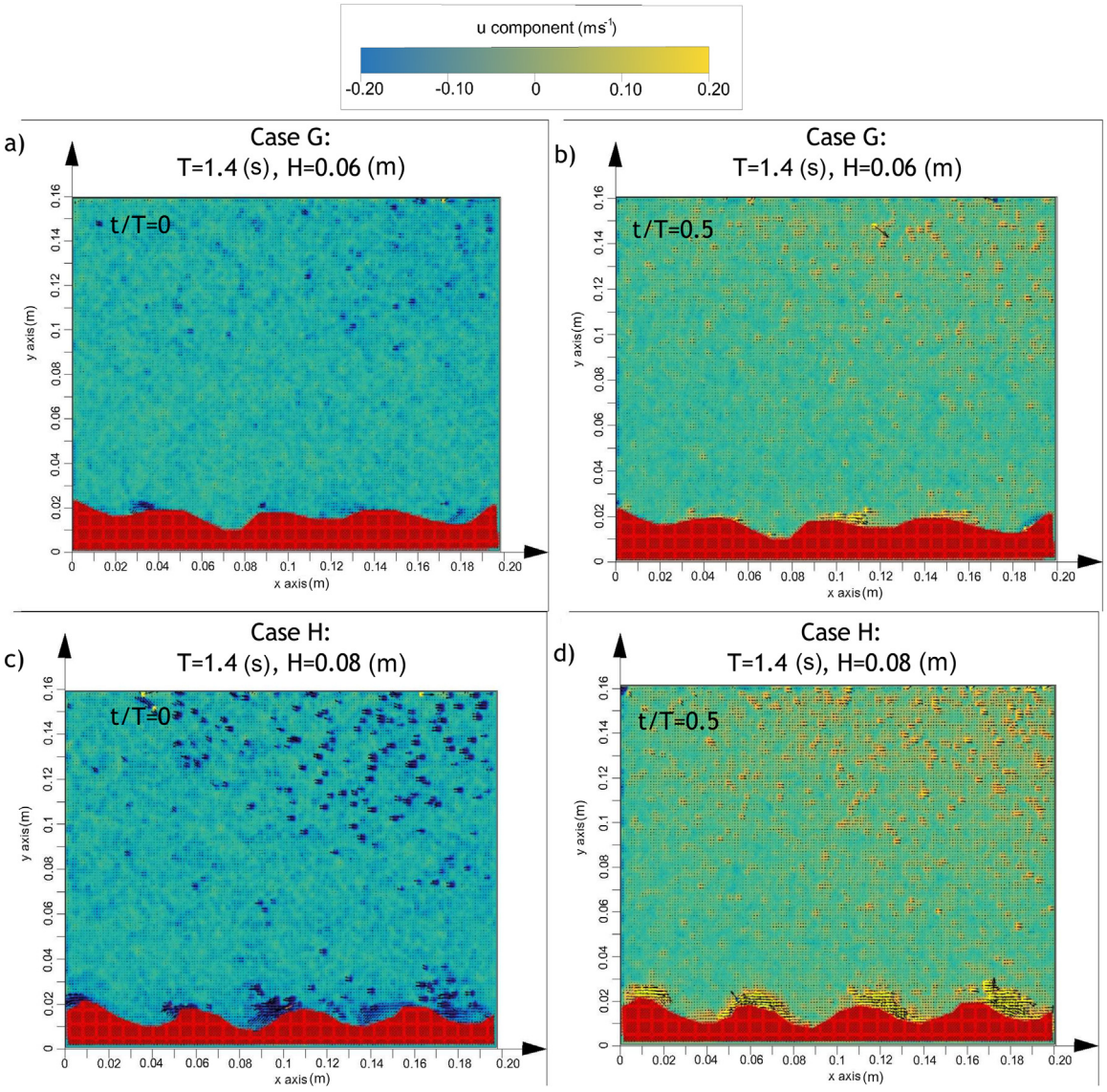

Figure 10 Instantaneous horizontal sediment velocity fields over a rippled bed for two cases of the wave height H and the wave period $T = 1.4$ s.

4.2. Sediment velocities due to surface waves of the period T = 1.4 s

Now we proceed to the results obtained for longer, more nonlinear, waves of the wave period $T = 1.4$ s. Two cases denoted by G and H and defined in Table 1, with the wave height H equal to either 0.06 or 0.08 m, respectively, were investigated in the flume. PIV images showing instantaneous horizontal velocity fields in the vicinity of a rippled bed for the two wave heights are displayed in Fig. 10. The images on the left correspond to the instant of a surface wave trough passage ($t/T = 0$) over the plotted area, while the analogous images on the right show velocities during the passage of a wave crest ($t/T = 0.5$).

The plots in the following figures illustrate sediment velocity profiles in the near-bed region determined for the two wave height cases. Fig. 11 presents horizontal velocity distributions along the horizontal profile over the ripples crests. The case of the smaller wave height ($H = 0.06$ m) is illustrated in Fig. 11a and b, showing that horizontal sediment velocities range from $u_s = -0.09$ m s^{-1} at the wave trough transition to about +0.11 m s^{-1} at a wave crest passage. The corresponding values of sediment velocities for the higher wave ($H = 0.08$ m) range from about -0.20 m s^{-1} at the wave trough transition to about +0.18 m s^{-1} at the wave crest transition, as is seen in Fig. 11c and d.

The plots in Fig. 12 illustrate the distributions of instantaneous horizontal sediment velocities along the vertical profile extending over a ripple crest (see Fig. 3). Fig. 12a shows velocities determined for the wave of the height $H = 0.06$ m. It is seen, for this particular data set, that the maximum near-bed sediment velocity magnitudes during a wave crest passage ($t/T = 0.5$, red lines) are equal to about 0.13 m s^{-1}, and those at the wave trough transition ($t/T = 0$, blue lines) are slightly larger and equal to about 0.15 m s^{-1}. Fig. 12b displays horizontal velocity profiles for the larger

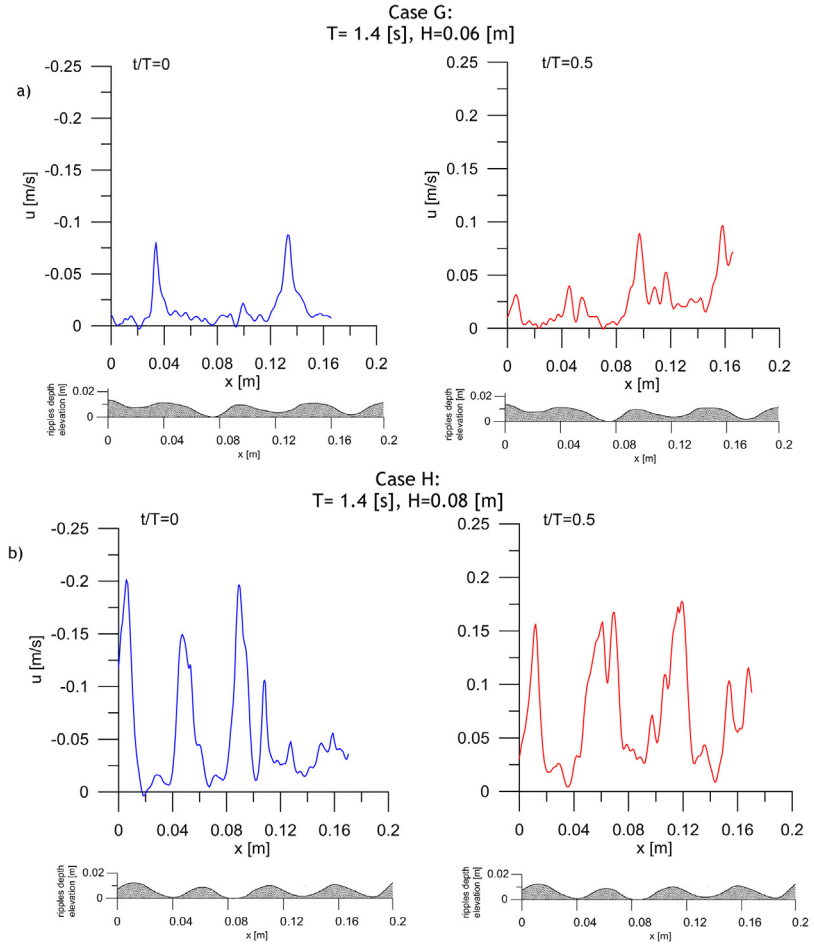

Figure 11 Instantaneous horizontal velocities of sediment grains along the horizontal profile over the bed ripples for two values of the wave height H and the wave period $T = 1.4\,\mathrm{s}$, at wave phases $t/T = 0$ (wave trough) and $t/T = 0.5$ (wave crest).

wave height $H = 0.08\,\mathrm{m}$. In this case, the near-bed sediment velocity magnitudes are equal to about $0.18\,\mathrm{m\,s^{-1}}$ at the wave crest transition, and $0.17\,\mathrm{m\,s^{-1}}$ at a wave trough passage. Again, it is observed (cf. Fig. 6) that the increase in the surface wave height significantly affects the thickness of the near-bed layer of intense sediment movement.

Fig. 13 displays variations in the vertical sediment velocity along the horizontal near-bed profile. Plots 13a and b, illus-

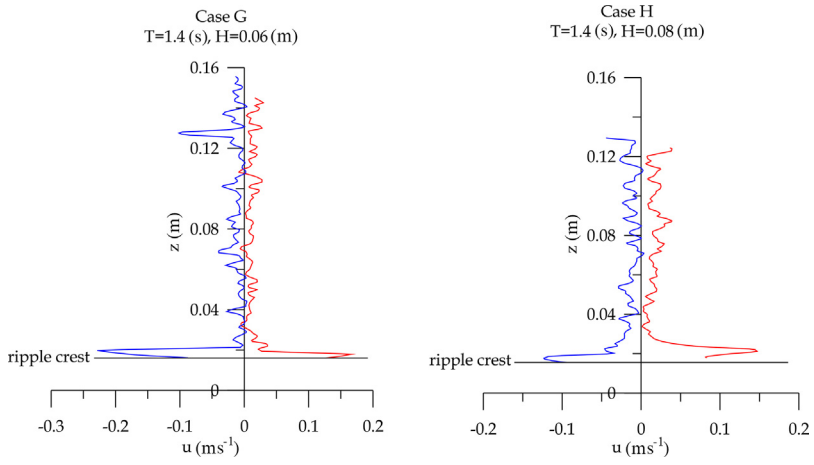

Figure 12 Instantaneous horizontal velocities of sediment grains along the vertical profile over a ripple crest for two values of the wave height H and the wave period $T = 1.4\,\mathrm{s}$, at wave phases $t/T = 0$ (wave trough transition, blue lines) and $t/T = 0.5$ (wave crest transition, red lines). (For interpretation of the references to color in this figure legend, the reader is referred to the web version of this article.)

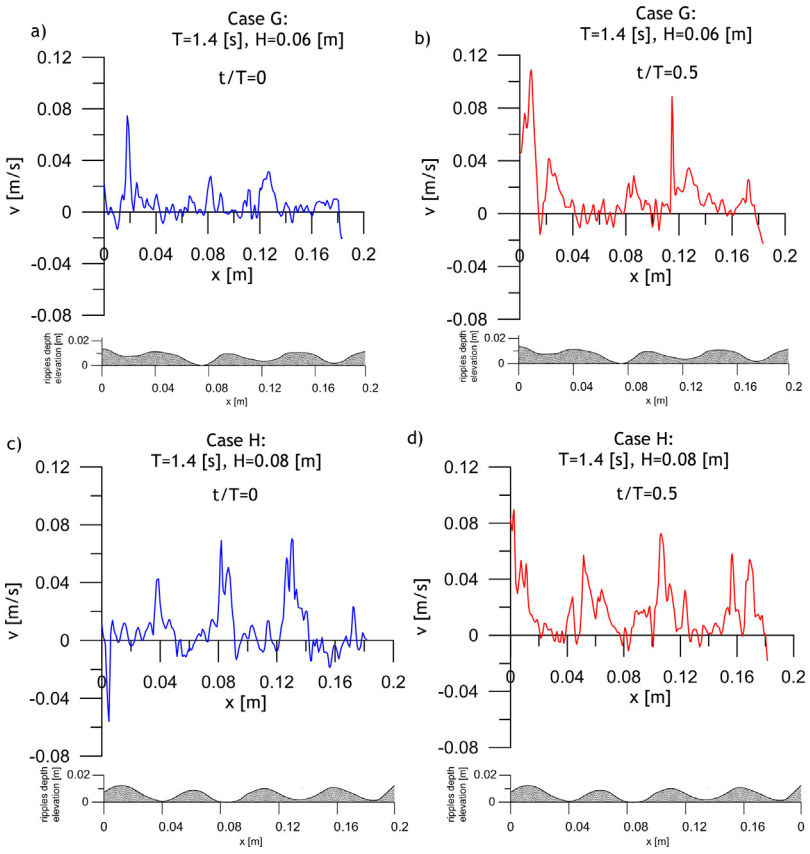

Figure 13 Instantaneous vertical velocities of sediment grains along the horizontal profile over the bed ripples for two values of the wave height H and the wave period $T = 1.4$ s, at wave phases $t/T = 0$ (wave trough) and $t/T = 0.5$ (wave crest).

trating the case of the smaller wave height $H = 0.06$ m, show velocities changing between 0.06 m s^{-1} and -0.03 m s^{-1} at the wave trough passage, and between 0.08 m s^{-1} and -0.03 m s^{-1} at the wave crest passage. The analogous values for the higher wave ($H = 0.08$ m), illustrated in Fig. 13c and d, range from about 0.07 m s^{-1} to -0.04 m s^{-1} at a wave trough passage, and from 0.08 m s^{-1} to -0.03 m s^{-1} at a wave crest passage.

Fig. 14 illustrates the distributions of sediment vertical velocities along the vertical profile extending over a ripple

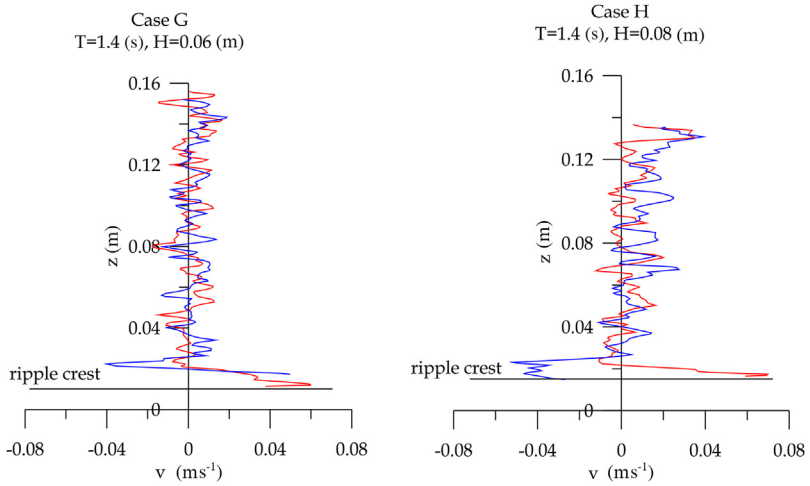

Figure 14 Instantaneous vertical velocities of sediment grains along the vertical profile over a ripple crest for two values of the wave height H and the wave period $T = 1.4$ s, at wave phases $t/T = 0$ (wave trough transition, blue lines) and $t/T = 0.5$ (wave crest transition, red lines). (For interpretation of the references to color in this figure legend, the reader is referred to the web version of this article.)

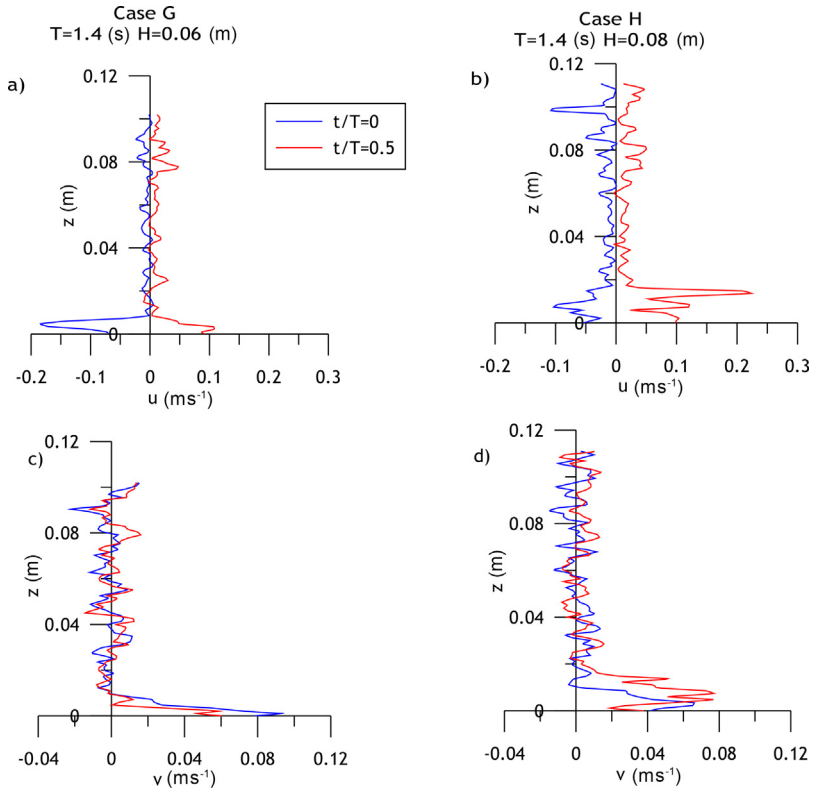

Figure 15 Instantaneous horizontal (plots a, b) and vertical (plots c, d) sediment velocities along the vertical profile over a ripple trough for three values of the wave height H and the wave period $T = 1.4$ s, at wave phases $t/T = 0$ (wave trough transition, blue lines) and $t/T = 0.5$ (wave crest transition, red lines). (For interpretation of the references to color in this figure legend, the reader is referred to the web version of this article.)

crest for the two wave heights. Comparing the plots for both cases with the corresponding plots in Fig. 12, one can note that the magnitudes of vertical sediment velocities in the near-bed turbulent layer are equal to about 1/3 of their horizontal counterparts.

Finally, Fig. 15 illustrates sediment velocity variation along the vertical profile located over a ripple trough. The two plots 15a and b show the distributions of horizontal velocities, and the corresponding plots 15c and d display vertical velocities.

5. Comparisons of experimental and analytical results

It is clearly seen in Figs. 5–9 and 11–15 that the spatial distributions of instantaneous sediment grain velocities are highly variable, reflecting complex physical mechanisms governing the movement of sediment grains in highly turbulent water flow in near-bed regions. First of all, the complexity of the phenomenon is due to the presence of vortices which cyclically appear and disappear near the slopes of bed ripples during successive phases of the oscillatory motion of water induced by surface waves, as described in detail by Van der Werf et al. (2007). In addition, the dynamic interactions of sediment grains with the bed (the mechanism of grain saltation), along with the interactions between grains suspended in water, all contribute to random fluctuations in sediment particle movements near the bed.

In this section, the empirical results from the flume are compared with results that can be obtained by applying analytical formulae presented in Section 2, describing velocity fields generated by surface waves of the Stokes type, the characteristics of the wave boundary layer, and the parameters (length and height) of bed ripples. Since the PIV technique fails to measure water particle velocities in the presence of sand grains suspended in water (because the latter are detected by this technique), water particle velocities are calculated analytically and then compared, in Section 5.1, with sediment grain velocities measured in the laboratory. In Section 5.2, the results from the flume experiments are compared with those known from the literature on sediment dynamics. Thus, the characteristics of the measured bedforms are compared with those predicted by the theory for given surface wave parameters, forces acting on sediment grains at the bed (expressed in terms of the Shields parameter) are evaluated, and the thicknesses of the wave-induced oscillating turbulent boundary layer (WBBL) are calculated and compared with those determined experimentally.

5.1. Sediment particle velocities versus water particle velocities

To compare the instantaneous velocities of sediment particles with those of water in the near-bed region, theoretical relations (1) and (2) describing second-order Stokes waves

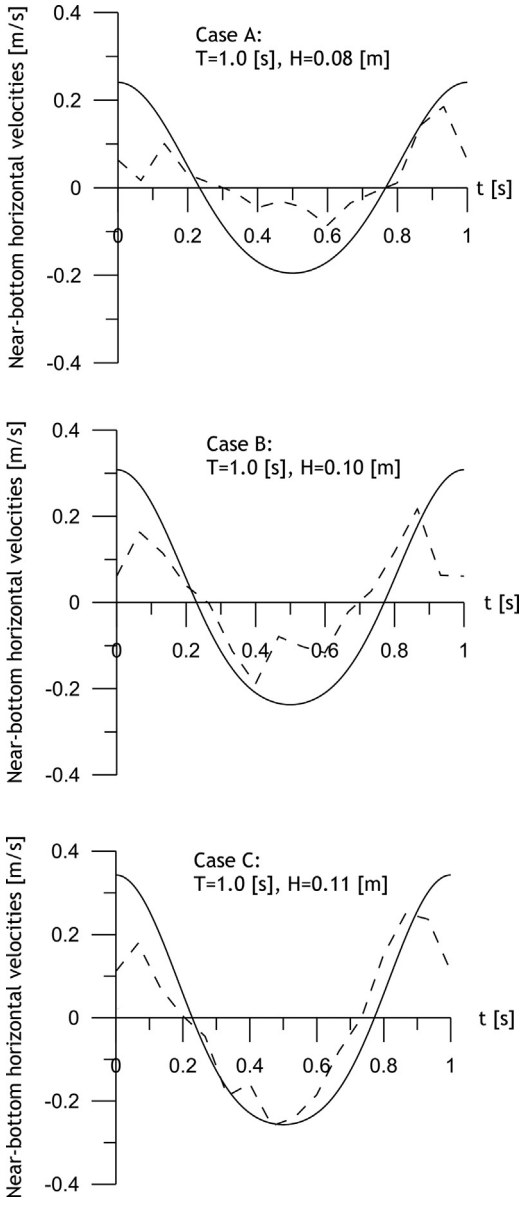

Figure 16 Variations in near-bed horizontal velocities of sediment particles (dashed lines) and water particles (solid lines) during one period of a surface wave for cases A, B and C ($T = 1.0$ s).

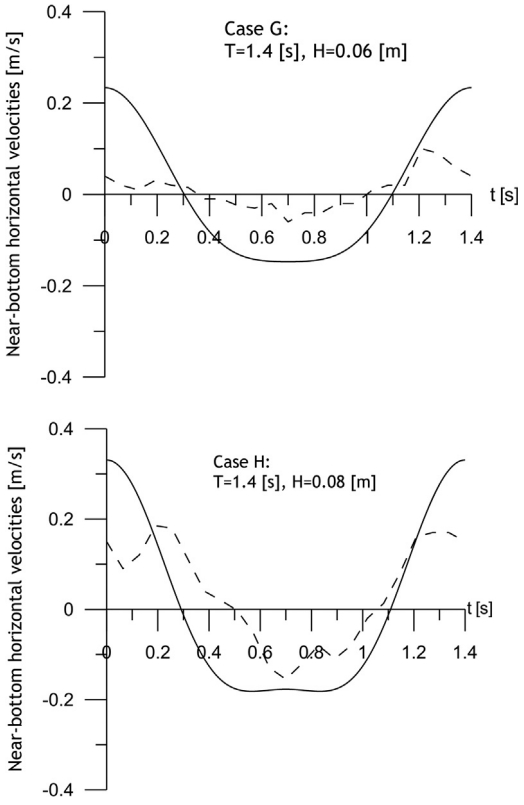

Figure 17 Variations in near-bed horizontal velocities of sediment particles (dashed lines) and water particles (solid lines) during one period of a surface wave for cases G and H ($T = 1.4$ s).

are employed. The plots in Figs. 16 and 17 display variations in the horizontal velocities of sediment and water particles at a point near a ripple crest point during the time of one wave period T. The plotted quantities for the sediment represent mean values calculated for a series of ten consecutive wave periods. Sediment velocities are plotted in the figures with an interval of 1/15 s, which is related to the frequency of 15 Hz at which successive images were recorded by the PIV system used in the experiments. This corresponds to only 16 time-points in the plots for the waves of the period $T = 1.0$ s, and 22 points for the waves with $T = 1.4$ s. The three cases (A, B and C) of waves with the period $T = 1.0$ s are illustrated in Fig. 16, with the solid lines showing water velocities, and the dashed lines representing sediment velocities. The corresponding plots for the longer waves, represented by cases G and H (of the period $T = 1.4$ s), are displayed in Fig. 17. In all the plots in Figs. 16 and 17, the instant $t = 0$ represents the time of a wave crest passage over a given point. It can be noted in the plots that the higher the wave height H, the higher the ratio of the horizontal velocity of sand grains to water velocity, u_s/u_w. For smaller wave heights (cases A and G), the ratios u_s/u_w, on average, do not exceed the values of about 0.3. On the other hand, for the higher and more non-linear waves, with the wave crests becoming shorter and the troughs becoming longer, the ratios u_s/u_w significantly increase during the wave trough passage. This is seen in the plots for cases C and H, representing the steepest waves investigated in the experiments, for which the above velocity ratios are, on average, as large as about 0.8 and more. This property is due to the fact that, for steep waves in shallow water, the trough passage phase lasts longer than the crest passage phase, so that there is more time for sediment particles to catch up with water during the trough phase of the oscillatory wave motion. This, in a way, also explains why the most intense changes in the sandy bedforms occur during the passage of wave troughs.

Fig. 18 illustrates time-variations in the vertical velocities of near-bed sediment particles versus wave-induced vertical water velocities defined by Eq. (2). Unlike the plots in Figs. 16 and 17, which show horizontal velocities at a point located on a ripple crest (at which vertical water velocities given by

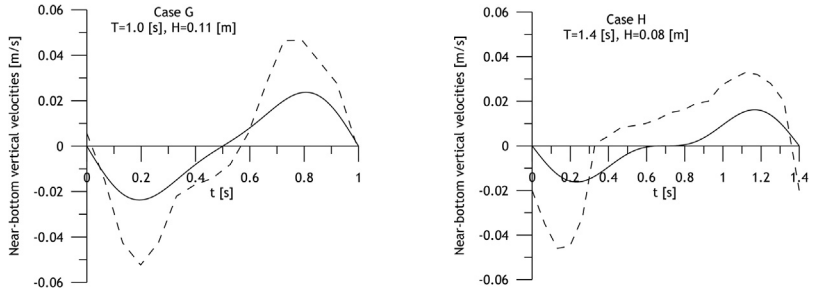

Figure 18 Variations in near-bed vertical velocities of sediment particles (dashed lines) and water particles (solid lines) during one period of a surface wave for cases C ($T = 1.0$ s, $H = 0.11$ m) and H ($T = 1.4$ s, $H = 0.08$ m).

Eq. (2) are zero), the plots in Fig. 18 show vertical velocities at a point directly above the middle of a ripple trough, at the ripple crest height. These plots illustrate cases C and H, representing the highest waves with the period 1.0 s and 1.4 s, respectively. It follows from the plots (see also Figs. 16c and 17b) that the maximum vertical velocities v_s of sediment particles at that point are about 20–25% of the maximum horizontal sediment velocities u_s at the neighbouring crest points. Unlike the maximum horizontal sediment velocities, which are equal to a fraction of the maximum water velocities, the maximum vertical sediment velocities considerably exceed the corresponding wave-induced water velocities. This effect, caused by the ejection of sand grains from the bed by ripple vortices, is particularly well pronounced for the longer wave represented by case H, which corresponds to the most non-linear wave analyzed in the experiments, see the Ursell and Reynolds number values listed in Table 1. It may be of interest to compare the maximum vertical velocities of sand grains, equal to about 0.05 m s^{-1}, with the grain settling velocity. It turns out that the latter, calculated from Eq. (17) in Section 2, is equal to 0.036 m s^{-1} for the sand grain diameter $d_{50} = 0.257$ mm.

The magnitudes of near-bed sediment grain and water velocities for the five wave cases investigated in the flume are compared in Table 2. For sediment, the numbers in the table represent time-averaged velocities calculated as means of extreme (both positive and negative) quantities over ten subsequent wave periods. The columns labelled u_s and u_w list the horizontal velocity magnitudes of sediment and water, respectively, at a wave crest passage, whereas those labelled $-u_s$ and $-u_w$ give the corresponding magnitudes at a wave trough passage over a given near-bed spatial point.

Finally, the plots in Fig. 19 show the dependence of the maximum near-bed sediment particle velocities on the value of the Shields parameter $\theta_{2.5}$ for the five wave cases investigated in the flume experiments.

5.2. Bed forms and wave bottom boundary layer thickness

In all surface wave cases investigated in the laboratory experiments described in this work, well-developed systems of regular bed ripples formed and remained stable in time. The characteristic geometric parameters of the ripples (their lengths λ_r and heights η_r) measured in the flume for the five cases considered are listed in Table 3. Given are the mean values and standard deviations (appearing after the signs $\pm$). The measured quantities, indicated by the suffix 'exp', are compared with corresponding quantities obtained from analytical formulae: (14) for λ_r and (15) for η_r, indicated by the suffix 'the'. In addition, the table also contains the values of the Shields parameter $\theta_{2.5}$ calculated from Eqs. (7) and (8). The last two columns in the table give the empirically and theoretically estimated depths δ of the wave bottom boundary layer, see Eqs. (11)–(13).

It is seen in the table that the empirically measured geometric parameters of the bed ripples are, in general, in good agreement with those predicted by the theory. In particular, the analytically determined ripple heights η_r fall within the range of values observed in the flume, except for case A, in which a small discrepancy (0.1 cm) has occurred. Regarding the ripple lengths λ_r, the agreement between empirically and theoretically evaluated values is seen for cases A, B and G, whereas for the most non-linear waves represented by cases C and H the observed ripple lengths are smaller than those given by the analytical formula.

As can be seen in Table 3, the values of the Shields parameter $\theta_{2.5}$ in our experiments varied between

Table 2 Magnitudes of near-bottom horizontal velocities of sediment and water particles for five surface wave cases considered.

Case	H [m]	T [s]	Water particles				Sediment particles			
			u_w [m s^{-1}]	$-u_w$ [m s^{-1}]	v_w [m s^{-1}]	$-v_w$ [m s^{-1}]	u_s [m s^{-1}]	$-u_s$ [m s^{-1}]	v_s [m s^{-1}]	$-v_s$ [m s^{-1}]
A	0.08	1.0	0.23	0.19	0.02	0.01	0.17	0.20	0.06	0.07
B	0.10	1.0	0.30	0.24	0.03	0.025	0.23	0.25	0.08	0.07
C	0.11	1.0	0.33	0.26	0.03	0.03	0.3	0.35	0.08	0.10
G	0.06	1.4	0.22	0.15	0.02	0.01	0.10	0.12	0.03	0.04
H	0.08	1.4	0.32	0.18	0.04	0.02	0.18	0.18	0.03	0.05

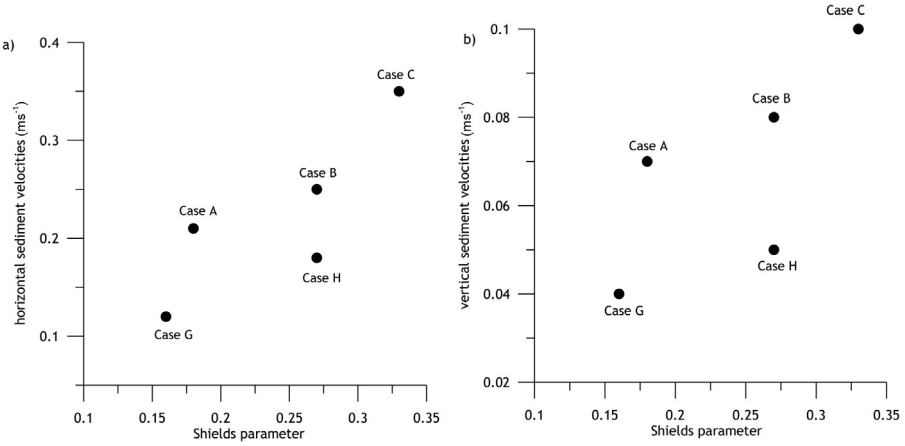

Figure 19 Maximum horizontal (a) and vertical (b) sediment near-bed velocities as functions of the Shields parameter $\theta_{2.5}$ for the five surface wave cases analyzed in the laboratory experiments.

Table 3 The values of the bed ripple length (λ_r), height (η_r), Shields parameter ($\theta_{2.5}$) and the thickness (δ) of the wave bottom boundary layer determined experimentally and theoretically for five surface wave cases considered.

Case	H [m]	T [s]	λ_r^{exp} [cm]	λ_r^{the} [cm]	η_r^{exp} [cm]	η_r^{the} [cm]	$\theta_{2.5}$ [–]	δ^{exp} [cm]	δ^{the} [cm]
A	0.08	1.0	3.5 ± 0.4	3.5	0.9 ± 0.1	0.71	0.18	1.5	2.31
B	0.10	1.0	4.1 ± 0.2	4.2	0.8 ± 0.1	0.80	0.27	3	3.58
C	0.11	1.0	3.7 ± 0.3	4.5	0.8 ± 0.1	0.81	0.33	4	4.01
G	0.06	1.4	5.4 ± 0.5	5.1	1.0 ± 0.2	0.92	0.16	2.5	3.12
H	0.08	1.4	5.1 ± 0.2	6.2	1.1 ± 0.1	1.02	0.27	4	4.92

0.16 and 0.33, which confirms that the range of $0.1 \leq \theta_{2.5} \leq 0.3$, approximately, corresponds to a stable system of bed forms, as was observed during the experiments.

With regard to the values of the wave bottom boundary layer thicknesses δ observed in the laboratory for the five wave cases investigated, they are in reasonable agreement with the corresponding values determined analytically.

6. Conclusions

The paper presents the results of laboratory measurements of surface wave-induced sediment movement over a mildly inclined rippled seabed carried out in a flume. The flow conditions investigated in the experiments corresponded to non-linear waves of the Stokes type with the Ursell number ranging from about 18 to about 39 for wave parameters selected for the measurements. For the fine sand used in the experiments, with the median diameter d_{50} = 0.257 mm, grain mobility numbers varied between 12 and 26. The near-bed water velocities generated by surface waves propagating in the flume resulted in the formation of a stable system of ripples with heights between approximately 0.7 and 1.2 cm and Shields parameter values between 0.18 and 0.33.

For the above-described flow conditions, the near-bed layer of intense sediment grain movements had a thickness of about 2–3 ripple heights above ripple crests, depending on the surface wave height. The maximum magnitudes of horizontal sediment velocities measured over ripple crests were about twice as large as those over ripple troughs. The maximum vertical sediment velocities measured above ripple crests and troughs were similar, amounting to approximately 1/4 to 1/3 of horizontal velocities over ripple crests.

It was found out during the laboratory experiments that sand grain velocities were successfully measured by the PIV method in a region extending a few centimetres over the bed, where the sediment concentration is the highest, and no seeding, which is commonly used in PIV measurements, was necessary. Above this layer, with decreasing concentration of sediment particles in water, the PIV system failed to distinguish sediment grains from water particles. For this reason, i.e. the inability of the PIV equipment to uniquely determine water particle velocities, water particle velocities were evaluated by analytical formulae in order to compare them with measured sediment grain velocities. Such comparisons showed that near-bed grain horizontal velocities were 1/3 to 1/2 of the corresponding water velocities, whereas maximum sediment grain vertical velocities exceeded those of water.

As mentioned in Introduction, the subject of this paper is very close to that considered in an earlier paper by Stachurska and Staroszczyk (2016), in which wave-induced flow over a horizontal sandy bed was analyzed in a flume. Horizontal velocity profiles in the two flow configurations were compared, but no clear qualitative differences were found between the flows over the horizontal bed and the bed inclined at 2%, bearing in mind the scatter in the measured data.

The laboratory measurements carried out in the flume produced detailed data sets containing the velocities of sediment grains above the rippled bed recorded for a series

of wave-induced oscillatory flows. These data sets can be used to test numerical models for simulating suspended sediment dynamics. One such model is being currently developed by the authors of this work.

Acknowledgements

Financial support for this research was provided by the National Science Centre (NCN), Poland, under contract no. UMO-2013/11/B/ST8/03818. The authors thank Dr Marek Szmytkiewicz, Associate Professor at the Institute of Hydro-Engineering of the Polish Academy of Sciences in Gdańsk, for his constructive comments which greatly helped to improve an early version of this paper. We are also grateful to two anonymous reviewers for their valuable comments on this manuscript.

References

Ahmed, A.S.M., Sato, S., 2001. Investigation of bottom boundary layer dynamics of movable bed by using enhanced PIV technique. Coast. Eng. 43 (4), 239–258, http://dx.doi.org/10.1142/S0578563401000360.

Alsina, J.M., Caceres, I., Brocchini, M., Baldock, T.E., 2012. An experimental study on sediment transport and bed evolution under different swash zone morphological conditions. Coast. Eng. 68, 31–43, http://dx.doi.org/10.1016/j.coastaleng.2012.04.008.

Bagnold, R.A., 1946. Motion of waves in shallow water, interaction between waves and sand bottoms. Philos. Trans. R. Soc. Lond. A187, 1–15, http://dx.doi.org/10.1098/rspa.1946.0062.

Doering, J.C., Baryla, A.J., 2002. An investigation of the velocity field under regular and irregular waves over a sand beach. Coast. Eng. 44, 275–300, http://dx.doi.org/10.15142/T3ZP4F.

Fenton, J.D., 1990. Nonlinear wave theories. Sea 9 (1), 3–25.

Fredsoe, J., 1984. Turbulent boundary layer in wave-current motion. J. Hydraul. Res. 110 (8), 1103–1120, http://dx.doi.org/10.1061/(ASCE)0733-9429(1984)110:8(1103).

Fredsoe, J., Deigaard, R., 1992. Mechanics of Coastal Sediment Transport. World Scientific Publ., Singapore, 392 pp., http://dx.doi.org/10.1142/1546.

Grant, W.D., Madsen, O.S., 1979. Combined wave and current interaction with a rough bottom. J. Geophys. Res 84, 1797–1808, http://dx.doi.org/10.102/JC084iC04p01797.

Grant, W.D., Madsen, O.S., 1982. Movable bed roughness in unsteady oscillatory flow. J. Geophys. Res. 87, 469–481, http://dx.doi.org/10.1029/JC087iC01p00469.

Hedges, T.S., 1995. Regions of validity of analytical wave theories. Proc. Inst. Civ. Eng. Water Marit. Energy 112, 111–114, http://dx.doi.org/10.1680/iwtme.1995.27656.

Inman, D., Bowen, A.J., 1962. Flume experiments of sand transport by waves and currents. Coast. Eng. Proc. 8, 137–150, http://dx.doi.org/10.1016/0378-3839(79)90019-X.

Nielsen, P., 1981. Dynamics and geometry of wave generated ripples. J. Geophys. Res. 86 (C7), 6467–6472, http://dx.doi.org/10.1029/JC086iC07p06467.

Nielsen, P., 1992. Coastal Bottom Boundary Layers and Sediment Transport. Advanced Series on Ocean Eng. World Scientific Publishing, Singapore, 340 pp., http://dx.doi.org/10.1142/1269.

Onoszko, J., 1965. Dynamics of a Sandy Seashore Profile Under the Action of Water Waves Normal to the Shoreline: Experimental Investigations. (Ph.D. thesis). Inst. Hydro-Eng. PAS, Gdańsk, Poland, (in Polish).

Ostrowski, R., 2004. Morphodynamics of a Multi-bar Coastal Zone. Instit. Hydro-Engineering PAS, Gdańsk, Poland, http://dx.doi.org/10.1515/heem-2016-0017.

Sato, S., Mimura, N., Watanabe, A., 1984. Oscillatory Boundary Layer Flow Over Rippled Beds. In: Proc. 19th Conf. Coast. Eng., Houston, 2293–2309, http://dx.doi.org/10.1061/9780872624382.155.

Stachurska, B., Staroszczyk, R., 2016. An investigation of the velocity field over rippled sand bottom. In: Proc. 6th IAHR IJREWHS, Lubeck, Germany, 122–131, http://dx.doi.org/10.15142/T3ZP4F.

Thielicke, W., Stamhuis, E.J., 2014. PIVlab – towards user-friendly, affordable and accurate digital Particle Image Velocimetry in MATLAB. J. Open Res. Software, http://dx.doi.org/10.5334/jors.bl.

Umeyama, T., 2012. Eulerian–Lagrangian analysis for particle velocities and trajectories in a pure wave motion using particle image velocimetry. Phil. Trans. R. Soc. A 370, 1687–1702, http://dx.doi.org/10.1098/rsta.2011.0450.

Ursell, F., 1953. The long-wave paradox in the theory of gravity waves. Math. Proc. Camb. Philos. Soc. 49 (4), 685–694, http://dx.doi.org/10.1017/S0305004100028887.

Van der Werf, J.J., Doucette, J.S., O'Donoghue, T., Ribberink, J.S., 2007. Detailed measurements of velocities and suspended sand concentrations over full-scale ripples in regular oscillatory flow. J. Geophys. Res. 112, F02012, http://dx.doi.org/10.1029/2006JF000614.

Willert, C.E., Gharib, M., 1991. Digital particle image velocimetry. Orig. Exp. Fluids 10, 181–193, http://dx.doi.org/10.1007/BF00190388.

Yang, B., Wang, Y., Liu, J., 2011. PIV measurements of two-phase velocity fields in aeolian sediment transport using fluorescent tracer particles. Measurement 44, 708–716, http://dx.doi.org/10.1016/j.measurement.2011.01.007.